

# Micro abrasion-corrosion of AISI 316L stainless steel

J.O. Bello, R.J.K. Wood and J.A. Wharton

*Surface Engineering and Tribology Group, School of Engineering Sciences,  
University of Southampton, Highfield, Southampton,  
SO17 1BJ, United Kingdom.*

## **Abstract**

In this study, the synergistic effects of abrasion and corrosion on AISI 316L stainless steel have been investigated using a micro-abrasion test rig. A series of results from abrasion-corrosion tests conducted using the micro-abrasion rig are presented. AISI 316L stainless steel has been studied under both pure abrasion and abrasion-corrosion conditions simulated by either distilled water or 3.5% sodium chloride based silicon carbide slurries. Tests have been conducted at various solids concentrations and for various sliding distances to enable the interactions between abrasion and corrosion to be better understood. The synergistic effect has been quantified and related to the material composition and the grooving or rolling abrasive wear mechanisms present. The synergistic levels were typically positive and have been discussed in terms of their dependence on the integrity of the passive films and the repassivation kinetics.

**Keywords:** *Abrasion-corrosion; Stainless steels; Synergy; Wear map*

## **1. Introduction**

In selecting materials for engineering applications, especially in conditions where corrosion is an issue, stainless steels usually receive greater preference over other metals due to their inherent corrosion resistance properties. However, when such applications involve sliding against other materials, a combination of mechanical (abrasion) and electrochemical (corrosion) processes takes place, termed abrasion-corrosion. In this context, abrasion-corrosion will be defined as the mechanical abrasion of a metal surface and the subsequent deterioration of the metal by the combined influence of corrosion and mechanical damage. The combined effect of abrasion and corrosion can lead to greater damage than simply the summation of the two parts and as a result can considerably shorten service life of components. Research interest in the abrasive and abrasive-corrosive properties of stainless steels has increased considerably in recent times. For example, some authors have studied the abrasive wear of some stainless steel grades [1-3]. Oscar et al. using the micro-abrasion ball-cratering test showed that abrasive wear performance of AISI 304 stainless steel is strongly influenced by the post-manufacture treatment applied to the sample [1]. Their results show that samples that were chemically treated wear at a rate approximately 25% faster than those that the cooling rates were carefully controlled. Similarly, other authors have also investigated the abrasive wear of laser-produced stainless steels and 304L with emphasis on metallurgical and micro-mechanical properties of the materials [2,3].

Significant effort has been undertaken into developing a greater understanding of the abrasion-corrosion properties of stainless steels for a range of different applications [4-12]. Of significant importance is the role of depassivation and repassivation of stainless steels during wear-corrosion. Sasaki and Burstein [13] in their study have shown that there is direct proportionality between depassivation and impact energy of the solid particles in the slurry, which subsequently leads to increased corrosion rate. It was also observed that the typical repassivation time during erosion-corrosion is in the range of 1 – 5 ms depending on the experimental conditions [13].

Garcia et al, adopting a ball-on-disc (stainless steel disc against an alumina ball) test method, have studied the integrity of passive films on the abrasion-corrosion of AISI 316 in the presence of a 0.5 M H<sub>2</sub>SO<sub>4</sub> solution [5]. Their results show that no breakdown of passive film occurred at loads below to 2 N, and the wear rate of AISI 316 stainless steel was similar to the wear rate when the sample was not immersed. However, between 2 and 12 N, removal of the passive oxide film on the AISI 316 sample resulted from a mechanism of periodic delamination of the oxide by the mechanical effect of the Alumina ball, with subsequent re-growth of the passive oxide film in the delaminated area [5]. Above 12 N, a relationship between the thickness of the passive oxide film and wear rate could not be established because wear of the parent bulk material dominated.

Thomann compared the wear-corrosion properties of two biocompatible stainless steels, 316L and Rex 734, used for biomedical applications, with specially developed alloy steel (P558) and found that, although the P558 alloy is not cheap to make, it has superior wear resistance and mechanical properties [6]. Dearnley suggested an alternative way of improving the resistance of 316L stainless steel to surface degradation by applying thin hard coatings [7]. However, the practicality of this procedure is thought to be fraught with difficulties due to the complex nature of the pervading corrosion-wear mechanisms [7]. Other techniques have been used to study the abrasion-corrosion of stainless steels [8,10]. Ferrer et al. used acoustic emissions (AE) to study the abrasion-corrosion of AISI 304L stainless steel in saline solution and concluded that in acidified saline environment, a pseudo-passive regime existed where synergy between abrasion and corrosion was observed, and that this depended strongly on the angle of impact for the lower wear rates but independent of angle of impact when the wear rate is significant [10]. A table summarising the different test methods, typical wear rates and test conditions previously used by other authors are presented in Table 1.

Unfortunately, despite the considerable effort that has been invested into understanding the abrasion-corrosion of stainless steels, it appears that little attention has been given to the role synergy plays during abrasion-corrosion. In-depth understanding of the subject of abrasion-corrosion cannot be achieved without a clearer view of the role of synergy. It is therefore the aim of this paper to further clarify the important role synergy plays in the understanding of the abrasion-corrosion of a grade of stainless steels, AISI 316L, using the micro-abrasion test method. Attempt will be made to highlight the effect of depassivation and repassivation of AISI 316L stainless steel on synergy. Therefore, using the Adachi and Hutchings [14] wear model as a starting point to establish abrasive severities over a range of abrasive concentrations, effort will be made to (1) quantify the amount of synergy involved during abrasion-corrosion tests, (2) establish the nature of the synergy and its physical meaning.

## **2. *Experimental details***

The experimental study consists of two tests using two different slurries: Pure abrasion (PA) test with the slurry made of silicon carbide (SiC) grit mixed with distilled water and abrasion-corrosion (AC) test with slurry made of SiC abrasive grit mixed with 3.5 % (0.6M) sodium chloride (NaCl) solution.

### **2.1 *Sample preparation***

The AISI 316L stainless steel was cut into test samples of 20 × 10 mm. The samples were polished in order to have a unified surface finish of ~ 1 μm. The samples were kept in a desiccator throughout the test programme. The abrasive slurry was prepared by mixing a known weight of dry F1200 SiC particles (~4.5 μm), see Figure 1, in 1 dm<sup>3</sup> of either distilled water or in 3.5% NaCl solution. The hardness of the abrasive particles was 2500 Hv. The hardness of the AISI 316L samples, measured using a standard Vickers' hardness tester, was ~175 Hv. The chemical composition of the AISI 316L test material is detailed in Table 2.

## 2.2 Methodology

The experiments were performed using a commercially available micro-abrasion test apparatus, the Phoenix Tribology TE66 Micro-Scale Abrasion Tester. A schematic diagram of the apparatus is shown in Figure 2. The AISI 316L sample was secured in the holder and loaded against the ball, which was held by friction and able to rotate parallel to the plane of the sample, while the slurry was drip-fed onto the ball at the rate of  $0.1 \text{ cm}^3/\text{s}$ . The geometry of the imposed wear scar was spherical. An alumina ( $\text{Al}_2\text{O}_3$ ) ball with a diameter of 22 mm was used as the counterface: surface roughness of  $\sim 1 \text{ }\mu\text{m}$  and hardness of 1100 Hv. To prevent the SiC abrasives from settling out the slurry was constantly agitated with the aid of a magnetic stirrer. The test conditions are detailed in Table 3. For each test condition, three measurements were made to ascertain the repeatability of the tests. Post-test analysis of the samples was conducted by a field emission gun scanning electron microscope (SEM).

## 2.3 The wear rate ( $k$ )

For micro-abrasion tests, the wear can be measured in two ways: either by measuring the displacement or depth of wear scar with respect to the machine frame using a transducer or alternatively the wear crater dimension (diameter) can be measured using a calibrated eyepiece. In this paper the latter method was used. The wear volume was calculated using an approximate formula, assuming the spherical cap geometry of the ball, Equation (1).

$$V \approx \frac{\pi b^4}{64R} \quad \text{for } b \ll R, \quad \dots\dots(1)$$

where  $V$ ,  $b$  and  $R$  are volume of wear, diameter of crater and radius of the ball respectively.. The specific wear rate,  $k$ , was estimated by dividing the wear volume from Equation (1) by the applied load,  $N$  and total sliding distance,  $L$ , see Equation (2).

$$V = kLN. \quad \dots\dots(2)$$

## 2.4 Potentiodynamic polarisation

Potentiodynamic polarisation measurements were carried out in a closed three-electrode cell in order to assess the corrosion behaviour of AISI 316L, with a sweep rate of  $0.2 \text{ mV / s}$  using a Gamry PC4-750 potentiostat and CMS100 software. The AISI 316L sample was secured in the electrochemical cell with  $1.1 \text{ cm}^2$  of the surface area exposed to be accessed by the test electrolyte, 3.5 % NaCl solution at  $20^\circ\text{C}$ . The counter electrode was graphite and the reference electrode a silver/silver chloride (Ag/AgCl) electrode.

## 3. Results and discussion

### 3.1 Wear mode mapping

The abrasives in the contact zone play a critical role on the nature of the wear during a micro abrasion test. They either roll (producing multiple indents) or slide causing grooving abrasion through micro ploughing. Adachi [14] has developed a principle to determine the wear regimes in which two-body grooving abrasion or three-body rolling abrasion is dominant. This is important because it allows an initial prediction of the mechanism. Figure 3 shows the wear mode map for all the abrasive concentrations used in this study. It can be seen that a region

exists called the mixed mode, which is where a combination of the two wear mechanisms can occur simultaneously.

$$S_c = \frac{W}{AvH^I} \quad \dots(3)$$

where  $S_c$  is the severity of contact,  $W$  is the applied load,  $A$  is the region over which the separation of the ball and the specimen is less than the diameter of the abrasive particle,  $v$  is the volume fraction of abrasives in slurry and  $H^I$  is the hardness ratio of the ball and specimen.

### 3.2 $k$ vs. volume fraction of abrasives

The pure abrasive and abrasive-corrosive wear tests on AISI 316L at a sliding distance of 180 m are shown in Table 4 and Figure 4. It can be seen that the specific wear rate increases with increasing abrasive volume fraction for both tests, which is an indication of direct proportionality between the two parameters. This is unexpected as the severity  $S_c$  decreases with increasing volume fraction. There is evidence that  $k$  is higher for all AC compared to PA tests except for the lowest volume fraction i.e. the two-body regime, suggesting that corrosive activities, and tribochemical wear, within the contact zone lead to more material removal than during mixed and three-body rolling abrasive wear. These results suggest that when the wear process moves from a two-body regime toward a three-body mode the wear damage is more severe. It is reasonable to assume that material removal during three-body wear, which is characterised by multiple indentations, is more efficient than two-body wear, usually associated with micro-ploughing. Figure 5 shows a similar series of tests for a sliding distance of 38 m which is also directly compared with that at 180 m. It can be seen that both results show a similar trend of an increase in  $k$  with increasing abrasive volume fraction. However,  $k$  for both PA and AC at 38 m was always higher than that at 180 m. To understand the reason for this behaviour, the effect of sliding distance (SD) on wear rate of AISI 316L was investigated. The results of  $k$  vs. SD in Figure 6 shows an initial marginal decrease in  $k$  as the SD decreases but tends towards a constant value as SD increases.

SEM inspection of the wear scars, both PA and AC, generated using 0.006 (two-body), 0.03 (mixed mode) and 0.135 (three-body) abrasive volume fractions are shown in Figures 7a to 7f. With increasing volume fraction of abrasive the predominant wear mechanism changes from two-body grooving to three-body rolling abrasion with multiple indents clearly evident. Under the AC conditions there appears to be greater surface roughness, see Figures 7d and 7f. This suggests the influence of the corrosive electrolyte results in additional damage with evidence of corrosion, possibly due to micro pitting type phenomena and work hardening surfaces leading to stress corrosion processes at areas of plastic deformation.

### 3.3 Corrosion measurement

Two separate corrosion tests were performed on AISI 316L in an effort to obtain the specific wear rate due to ‘corrosion’ only: (a) mechanical -  $\text{Al}_2\text{O}_3$  ball rotated against the AISI 316L sample with only the corrosive electrolyte (no SiC abrasive) and (b) electrochemical - polarisation of the stainless steel as described in Section 2.4 above.

#### 3.3.1 Alumina ball and no SiC abrasive

To establish the corrosion component under actual micro-abrasion conditions a series of tests were performed within the ball-cratering rig with no slurry only the 3.5 % NaCl solution. The scar diameter, resulting from the continual depassivation/stripping of the protective oxide film by tribocorrosion, i.e. the simultaneous mechanical wear, electrochemical oxidation and adhesive wear mechanisms, was assessed in the usual manner to give a specific wear rate of  $2.51 \times 10^{-14} \text{ m}^3 / \text{Nm}$  at 38 m and  $8.01 \times 10^{-14} \text{ m}^3 / \text{Nm}$  at 180 m.

### 3.3.2 Polarisation curve of AISI 316L stainless steel in 3.5 wt% NaCl

For stainless steels, pitting is a well-known phenomenon that takes place preferentially at sulphide inclusions, notably MnS, in the exposed metal surface [15-19]. Consequently, stainless steel pitting behaviour has been reported to depend on the most damaging sulphide inclusion; i.e. the largest inclusion [20]. Figure 8 shows the potentiodynamic curve for AISI 316L stainless steel when exposed to 3.5 % NaCl solution. Metastable pitting activity can be clearly seen as revealed by a series of transients in the scan from 0.000 V to the breakdown potential at +0.320 V. Metastable pitting on stainless steels can be observed at potentials below the pitting potential, or above the pitting potential before the start of stable pitting [20]. Overall, the corrosion performance of AISI 316L when compared with similar austenitic stainless steels, such as AISI 304, is generally related to the role of alloyed molybdenum; it is reported that the molybdenum changes the anodic dissolution kinetics of the active pit surface [21,22].

The corrosion current ( $I$ ) was determined from the polarisation curve using the Tafel extrapolation method. From the corrosion current, the mass loss for a given time can be calculated using Faraday's law on the assumptions that the metallic components of the alloy are oxidised to  $\text{Fe}^{2+}$ ,  $\text{Cr}^{2+}$ ,  $\text{Ni}^{2+}$  and  $\text{Mo}^{6+}$  during dissolution. For the given AISI 316L composition, the calculated equivalent oxidation state of the cations produced by dissolution is 2.2, with an equivalent atomic weight of 56.3 g / mol and density of 7.89 g / cm<sup>3</sup>. This resulted in a mass loss rate of  $5.20 \times 10^{-12}$  g / s. In order to assess the influence of corrosion during abrasion-corrosion the mass loss was converted into a specific wear rate, with both sliding distances (38 and 180 m, 760 and 3600 s respectively) giving a  $k$  of  $5.25 \times 10^{-17}$  m<sup>3</sup> / Nm. The  $k$  obtained from the polarisation test is small in comparison with typical  $k$  values using the Al<sub>2</sub>O<sub>3</sub> ball rotation and corrosive electrolyte. Ultimately, this will have an affect on the synergy analysis as discussed in Section 3.4.

### 3.4 The role of Synergy

Evaluating synergy during wear-corrosion process has been a subject of much debate [10,23]. Some authors have suggested that corrosion leads to increase abrasion resistance in some materials [10], while others hold the opposite opinion. The results of abrasion-corrosion tests seem to be dependent more on techniques and test conditions adopted during any test. However, the ASTM G119-93 [24] has given a general guideline for determining synergy during abrasion-corrosion test. In this paper we have attempted to evaluate synergy via three approaches, which have been used in the past by other authors. This allows proper comparisons to be made between different methods of estimating synergy. Mathematically, these terms are listed below:

$$S = T - W \quad \dots\dots(4)$$

$$S_1 = T - (W + C_1) \quad \dots\dots(5)$$

$$S_2 = T - (W + C_2) \quad \dots\dots(6)$$

Where  $C_1$  and  $C_2$ , are  $k$  for the Al<sub>2</sub>O<sub>3</sub> ball (Section 3.3.1) and polarisation (Section 3.3.2), and  $W$ ,  $T$ , and  $S$  are pure abrasion (PA), abrasion-corrosion (AC), and synergy, respectively. Gant et al. [25] have attempted to evaluate synergy of some hard metals using Equations (4) and (5) but have not considered Equation (6).

The simplest approach, Equation (4), is the most attractive, however, it does not accommodate the influence of corrosion. The research literature debates this as well and certain research groups have introduced  $C_2$  from polarisation curves made under static conditions. However, by their nature polarisation type approaches will consider the whole wetted surface as opposed to the small active wear scar area that is formed during the micro-abrasion test. The alternative approach is to attempt to generate  $C_1$  with ball rotation and no SiC abrasive. This is

likely to produce tribochemical wear but may also produce alumina asperity abrasion. With regard to the ASTM standard, in situ electrochemical measurements under dynamic situations are difficult to interpret [5].

The evaluated synergies for  $S$  and  $S_1$  are shown in Figures 9 and 10.  $S_2$  was not plotted on Figure 9 since  $C_2$  was very small ( $5.25 \times 10^{-17} \text{ m}^3 / \text{Nm}$ ) and as such has little overall effect on synergy. Thus, in this instance Equations (4) and (6) are practically the same. As outlined above  $C_2$  does not involve any mechanical input with the implication that the passive film is not damaged or removed to any great extent. However, in the case of  $C_1$ , the tribochemical wear and possibly  $\text{Al}_2\text{O}_3$  asperities continually remove the protective passive film exposing an active AISI 316L surface to the corrosive electrolyte. The  $S_1$  value emphasises the contribution of the SiC abrasives in the slurry to contact degradation.

At 38 m (Figure 9), for all three wear mechanisms there is positive synergy, the worst-case being for two-body at 20 to 30%, whilst for all other conditions there is a modest positive synergy. Conversely, at 180 m (Figure 10), two-body abrasion produced significant negative synergy between  $-13$  to  $-100\%$ . This behaviour maybe related to the longer test duration and thus corrosion can have more of an influence, probably reflecting differences in repassivation kinetics and/or composition of the passive film reducing the overall level of two-body abrasion.

Figure 11 compares  $S_1$  at both 38 and 180 m. There appears to be a significant difference in synergy at two-body and mixed mode region compared with synergy within the three-body region. Similar trends can be seen in Figures 9 and 10 where  $S$  and  $S_1$  show large differences between two-body and mixed mode regimes. This behaviour suggests that two-body abrasion is not very stable, less reproducible compared with three-body, and maybe difficult to control. This is confirmed by the experimental error shown for the two-body wear tests, see Figure 11. Rabinowicz et al. [26] in their study of abrasive wear under a three-body regime suggested that three-body abrasion leads to more reproducible test results compared with two-body. Batchelor and Stachowiak [23] have also suggested that rolling abrasion (three-body) is an effective way of removing passive film of corrosion products from a test material during abrasion-corrosion, although this was not observed in this study.

To establish the balance between mechanical and electrochemical degradation the data can be graphically represented on a mechanistic map where AC-PA (electrochemical processes/losses) is plotted vs. PA (mechanical processes/losses). As seen in Figure 12 the majority of the data is in the abrasion-corrosion regime where mechanical processes are less than  $10\times$  the electrochemical processes.

#### 4. Conclusions

- The specific wear rate changes as a function of abrasive volume fraction.
- Increasing sliding distance led to a decrease in specific wear rate.
- Abrasive particles will influence synergy. Corrosion rate obtained without abrasive particle led to about 70 – 80% decrease in the amount of synergy for tests at 38 m sliding distance.
- In this study, two-body abrasion shows more inconsistency than three-body for abrasion-corrosion evident by the relatively high error shown in the synergy.
- These interactive results are for AISI 316L under abrasion-corrosion where the ratio of AC-PA / PA is between 0.1 and 1.

#### Acknowledgements

The authors acknowledge the support of the School of Engineering Sciences, University of Southampton in undertaking this work.

## References

1. A. Oscar, R.S. Allan, S.K. Igor, S.C. Sergio, *Wear*, **257** (2004) 999–1005.
2. G. Abbas, U. Ghazanfar, *Wear*, **258** (2005) 258–264.
3. A. Van Herpen, B. Reynier, C. Phalipou, *Wear*, **249** (2001) 37–49.
4. M. Reza Bateni, J.A. Szpunar, X. Wang, D.Y. Li, Wear and corrosion wear of medium carbon steel and 304 stainless steel. *Wear*, in press.
5. I. Garcia, D. Drees, J.P. Celis, *Wear*, **249** (2001) 452–460.
6. I.U. Thomman, P.J. Uggowitzer, *Wear*, **239** (2000) 48–58.
7. P.A. Dearnley, G. Aldrich-Smith, *Wear*, **256** (2004) 491–499.
8. R. Oltra, B. Chapey, L. Renaud, *Wear* **186–187** (1995) 533–541.
9. C. Allen, A. Ball, *Wear*, **74** (1981 – 1982) 287–305.
10. F. Ferrer, H. Idrissi, H. Mazille, P. Fleischmann, P. Labeeuw, *NDT & E International*, **33** (2000) 363–371.
11. M-H. Hong, S-I. Pyun, *Wear*, **147** (1991) 69–78.
12. C-W. Wu, *Wear*, **162–164** (1993) 950–953.
13. K. Sasaki and G. T. Burstein, *Philosophical Magazine Letters*, 80 (2000) 489 – 493.
14. K. Adachi, I.M. Hutchings, *Wear*, **255** (2003) 23–29.
15. G. Wranglen, *Corros. Sci.*, 14 (1974) 331–349.
16. J.E. Castle, R. Ke, *Corros. Sci.*, 30 (1990) 409–428.
17. D.E. Williams, J. Stewart, P.H. Balkwill, *Corros. Sci.*, 35 (1994) 1213–1235.
18. P.C. Pistorius, G.T. Burstein, *Philos. Trans. R. Soc. London A341* (1992) 531–559.
19. J.A. Wharton, R.J.K. Wood, B.G. Mellor, *Corros. Sci.*, 45 (2003) 97–122.
20. J. Stewart, D.E. Williams, *Corros. Sci.*, 33 (1992) 457–463.
21. R. Ke, R. Alkire, *J. Electrochem. Soc.*, 142 (1995) 4056–4062.
22. G.O. Ilevbare, G.T. Burstein, *Corros. Sci.*, 43 (2001) 485–513.
23. A.W. Batchelor, G.W. Stachowiak, *Wear*, **123** (1988) 281–291.
24. ASTM G119-93, Standard guide for determining synergism between wear and corrosion, in: *ASTM Handbook*, 1998, pp. 529–534.
25. A.J. Gant, M.G. Gee, A.T. May, *Wear*, **256** (2004) 500–516.
26. E. Rabinowicz, L.A. Dunn, P.G. Russell, *Wear*, **4** (1961) 345–355.

## Tables

**Table 1:** Comparison between wear rates observed by other authors

<b>k (m<sup>3</sup>/Nm)</b>	<b>Load (N)</b>	<b>SD (m)</b>	<b>Abrasive type</b>	<b>Abrasive size</b>	<b>Test type</b>	<b>Steel type</b>	<b>Environment</b>	<b>Ref.</b>
$1.42 \times 10^{-13}$	0.32	10	Diamond	0.25 $\mu$ m	Pure wet abrasion	304	Distilled water	[1]
$7.0 \times 10^{-14}$	5.00	130	Without abrasive	N/A	Sliding wear - corrosion	316	H <sub>2</sub> SO <sub>4</sub> solution	[5]
$3.78 \times 10^{-14}$	1.39	1000	Sand	50-70 $\mu$ m	Erosion-Corrosion	316	NaCl solution	[6]

**Table 2:** Chemical composition of AISI 316L

	<b>Composition (wt%)</b>						
	<b>Cr</b>	<b>Ni</b>	<b>Mo</b>	<b>Mn</b>	<b>S</b>	<b>C</b>	<b>Fe</b>
AISI 316L – spec.*	16.0-18.0	10.0-14.0	2.0-3.0	2.0	0.03	0.03	Bal.
AISI 316L	16.41	10.10	2.07	1.30	0.008	0.02	Bal.

\*Single figures represent maximum values.

**Table 3:** Details of the experimental conditions

<b>Test conditions</b>	<b>Quantity</b>
Load (N)	0.25
Speed (m / s)	0.05
Temperature (°C)	25
Slurry conc. (g / cm <sup>3</sup> of distilled water)	0.006, 0.03, 0.072, 0.135, 0.238
Slurry feed rate (cm <sup>3</sup> / s)	0.1
Sliding distance (m)	38, 180
Counterface material	Al <sub>2</sub> O <sub>3</sub>
Corrosive electrolyte	3.5% NaCl solution

**Table 4:** Specific wear rates vs. volume fraction of SiC abrasive.

<b>SiC abrasive volume fraction</b>	<b>Specific wear rate, <math>k</math> (m<sup>3</sup> / Nm)</b>					
	<b>PA</b>	<b>38 m AC</b>	<b>C<sub>1</sub></b>	<b>PA</b>	<b>180 m AC</b>	<b>C<sub>1</sub></b>
0.006	$1.98 \times 10^{-13}$	$2.82 \times 10^{-13}$	$2.51 \times 10^{-14}$	$1.06 \times 10^{-13}$	$9.36 \times 10^{-13}$	$8.01 \times 10^{-14}$
0.030	$4.21 \times 10^{-13}$	$4.63 \times 10^{-13}$	$2.51 \times 10^{-14}$	$1.23 \times 10^{-13}$	$2.30 \times 10^{-13}$	$8.01 \times 10^{-14}$
0.072	$7.83 \times 10^{-13}$	$9.92 \times 10^{-13}$	$2.51 \times 10^{-14}$	$4.89 \times 10^{-13}$	$6.09 \times 10^{-13}$	$8.01 \times 10^{-14}$
0.135	$1.36 \times 10^{-12}$	$1.44 \times 10^{-12}$	$2.51 \times 10^{-14}$	$9.87 \times 10^{-13}$	$1.19 \times 10^{-12}$	$8.01 \times 10^{-14}$
0.238	$1.58 \times 10^{-12}$	$1.70 \times 10^{-12}$	$2.51 \times 10^{-14}$	$1.25 \times 10^{-13}$	$1.51 \times 10^{-13}$	$8.01 \times 10^{-14}$

## Figures

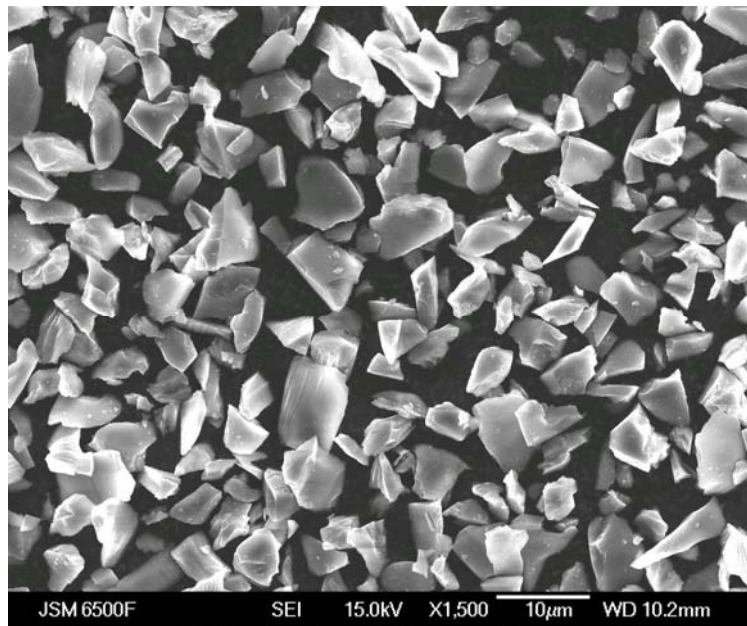


**Figure 1:** SEM of SiC abrasives used in the slurry, the mean particle size of the abrasives was  $\sim 4.5 \mu\text{m}$ .

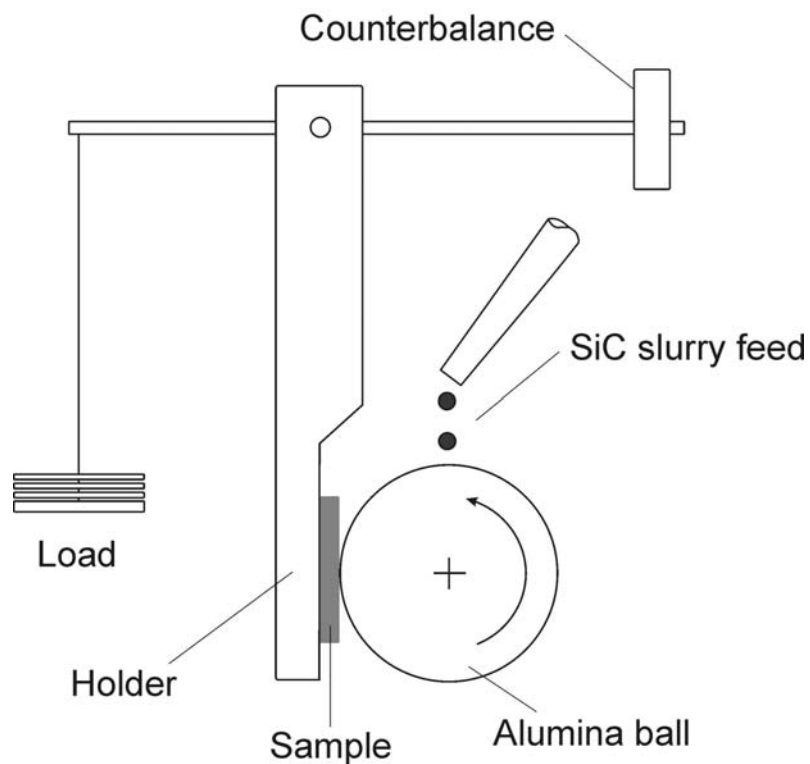


**Figure 2:** Schematic of the micro-abrasion ball-cratering test rig.

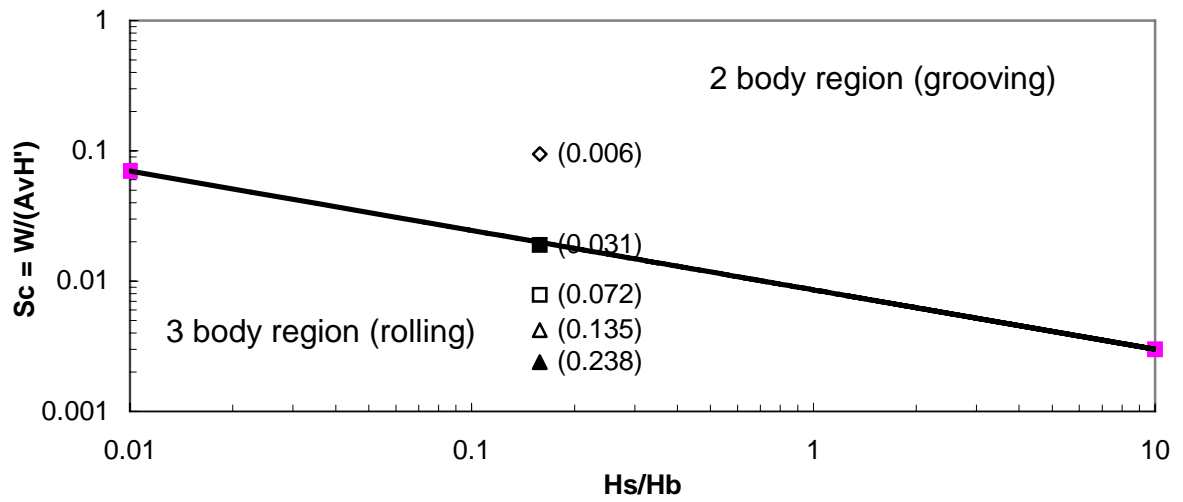


**Figure 3:** Wear mode mapping of all the abrasive concentrations used for the slurry tests on AISI 316L stainless steel.  $Sc$  is severity of contact.

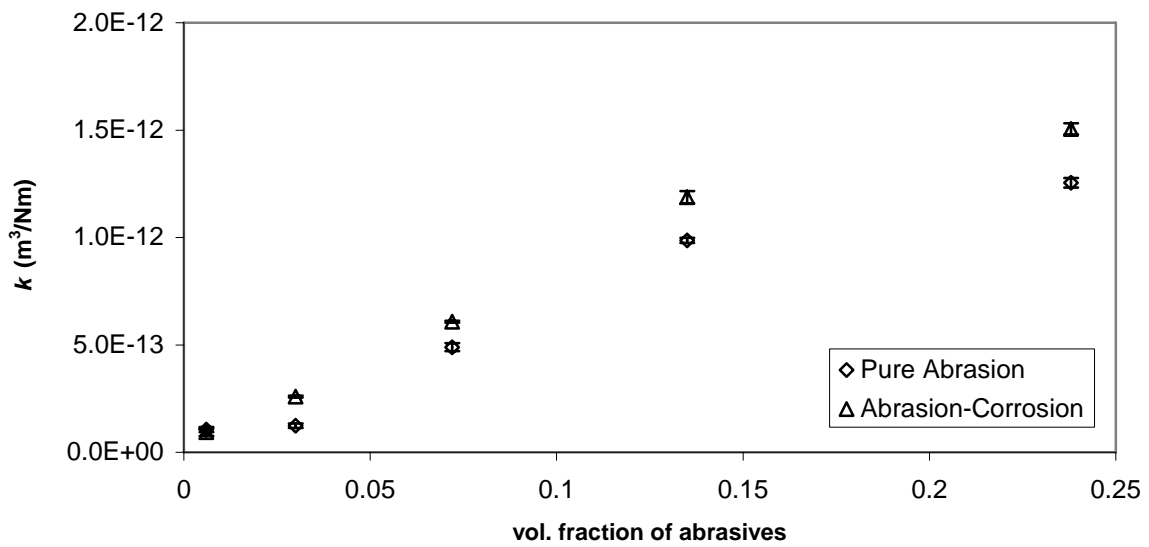


**Figure 4:** Specific wear rates for abrasion and abrasion-corrosion on AISI 316L for a sliding distance of 180 m.

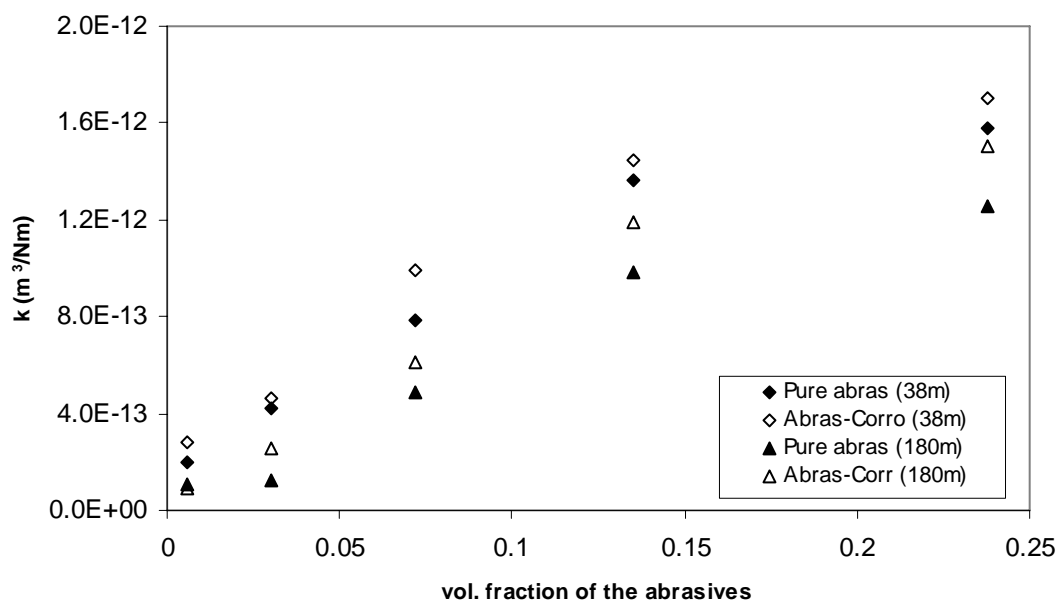


**Figure 5:** Comparison between the abrasion and abrasion-corrosion of AISI 316L stainless steel at sliding distances of 38 and 180 m.

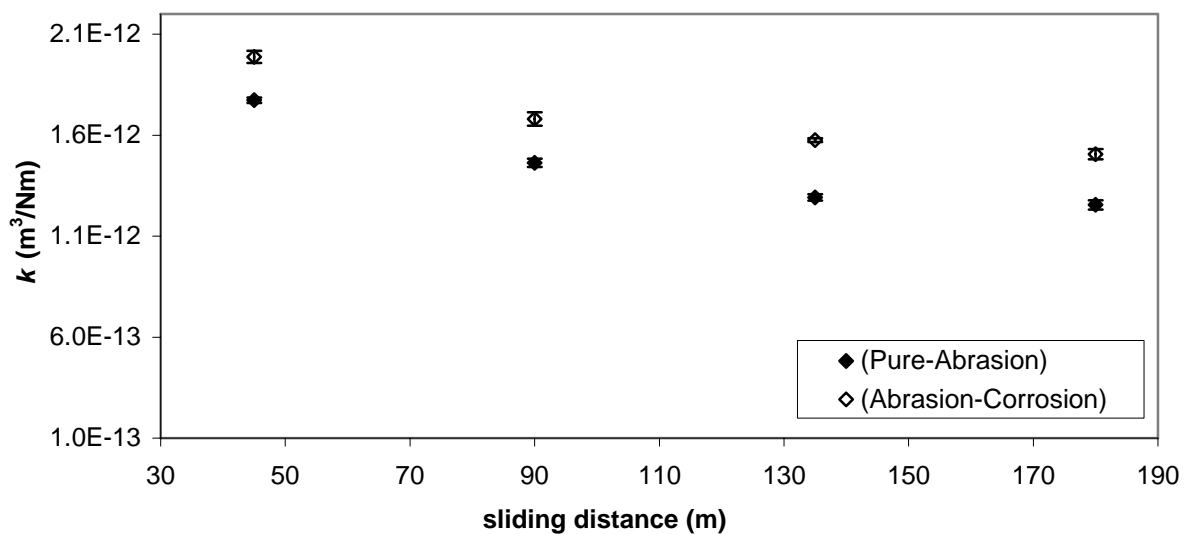


**Figure 6:** Specific wear rates vs. SD for AISI 316L at a 0.238 abrasive volume fraction under three-body rolling abrasion.

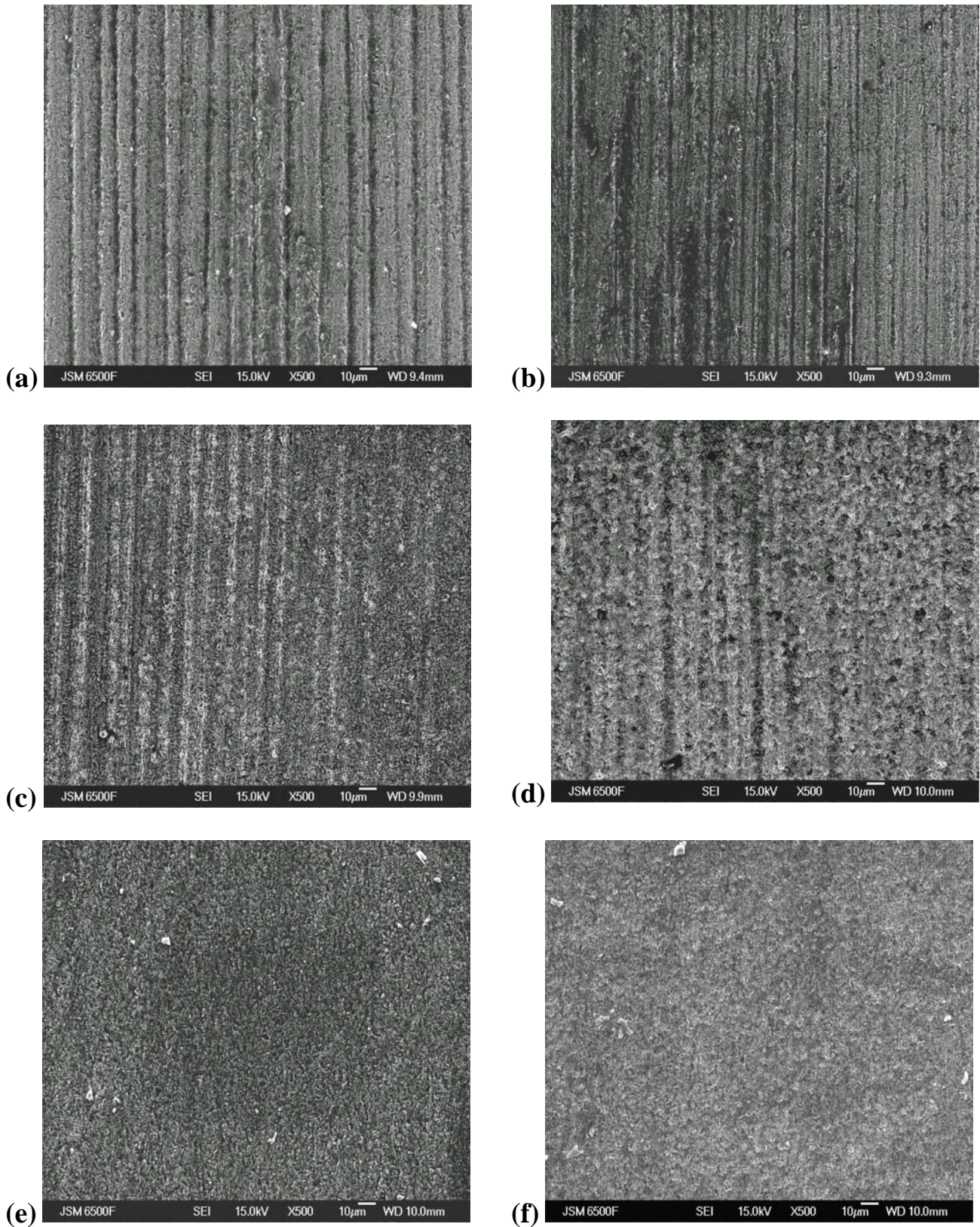


**Figure 7:** SEM micrographs of micro-abrasion scars after 180 m sliding: (a) 0.006 volume fraction for PA, (b) 0.006 volume fraction for AC, (c) 0.03 volume fraction for PA, (d) 0.03 volume fraction for AC, (e) 0.135 volume fraction for PA and (f) 0.135 volume fraction for AC.

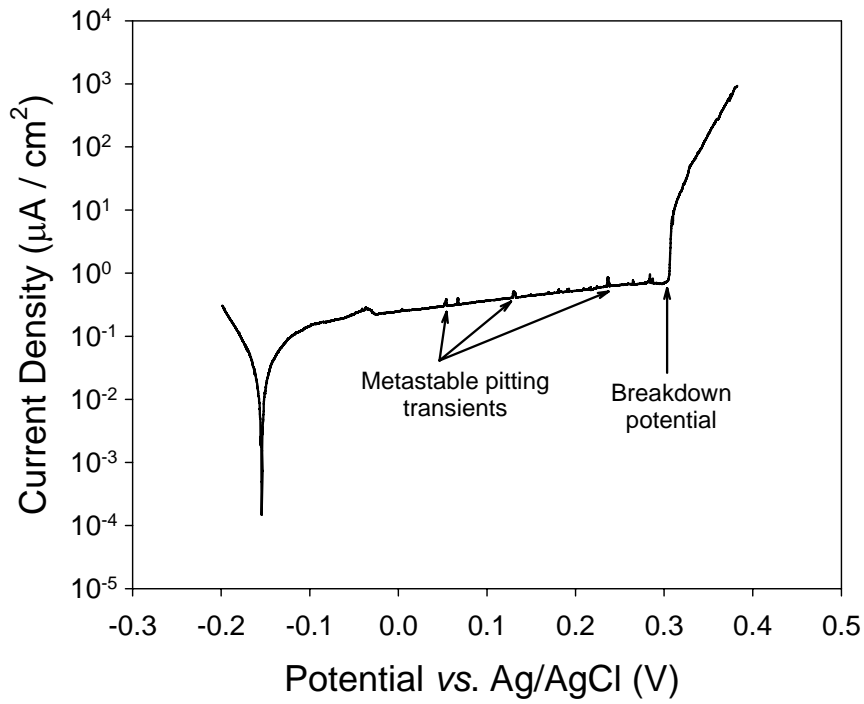


**Figure 8:** Potentiodynamic polarisation of AISI 316L in 3.5% NaCl solution (sweep rate: 0.2 mV/s).

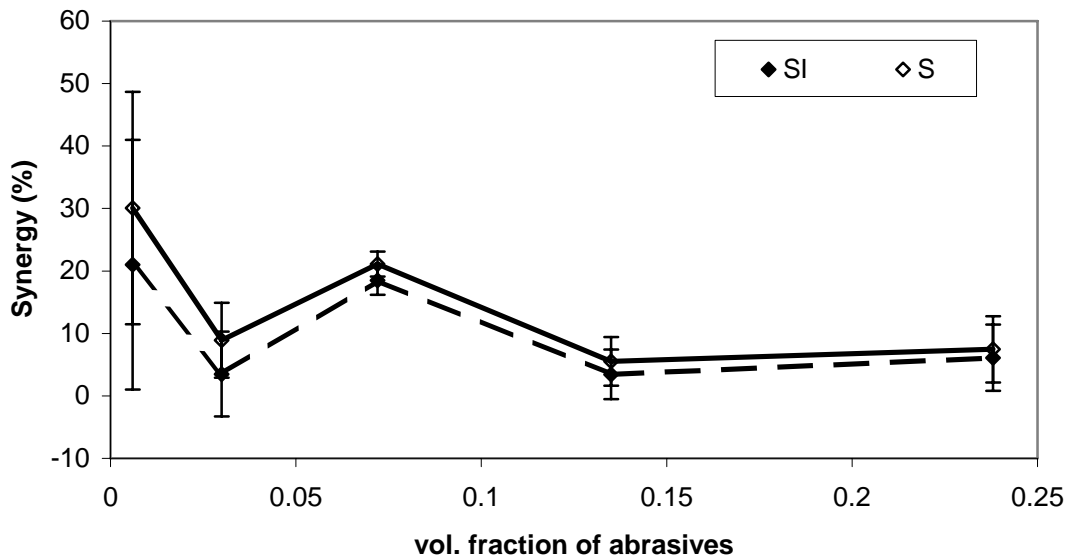


**Figure 9:** Synergy (%) vs. abrasive volume fraction for a sliding distance of 38 m.

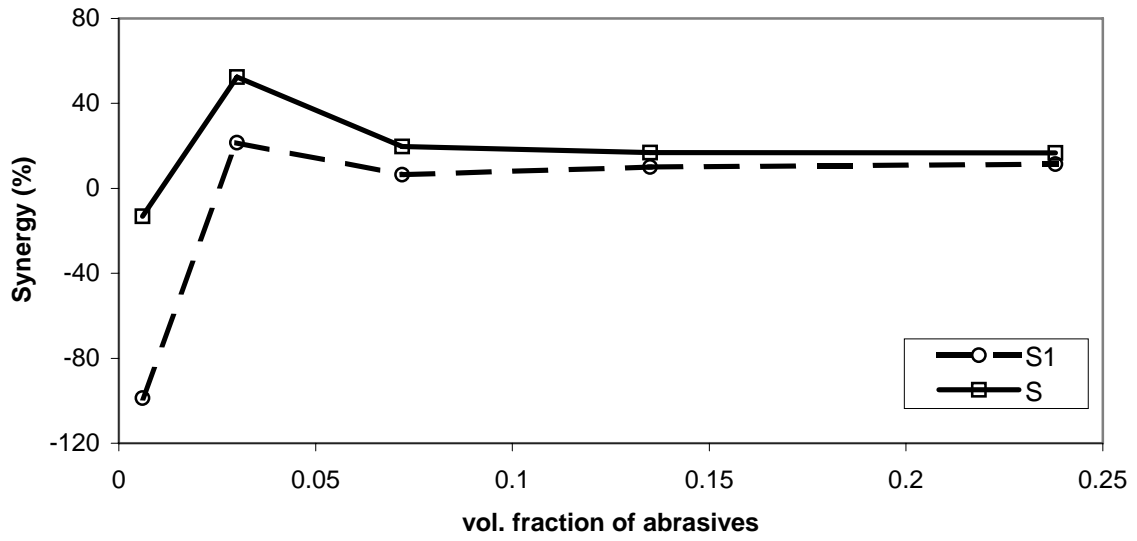


**Figure 10:** Synergy (%) vs. abrasive volume fraction for a sliding distance of 180 m.

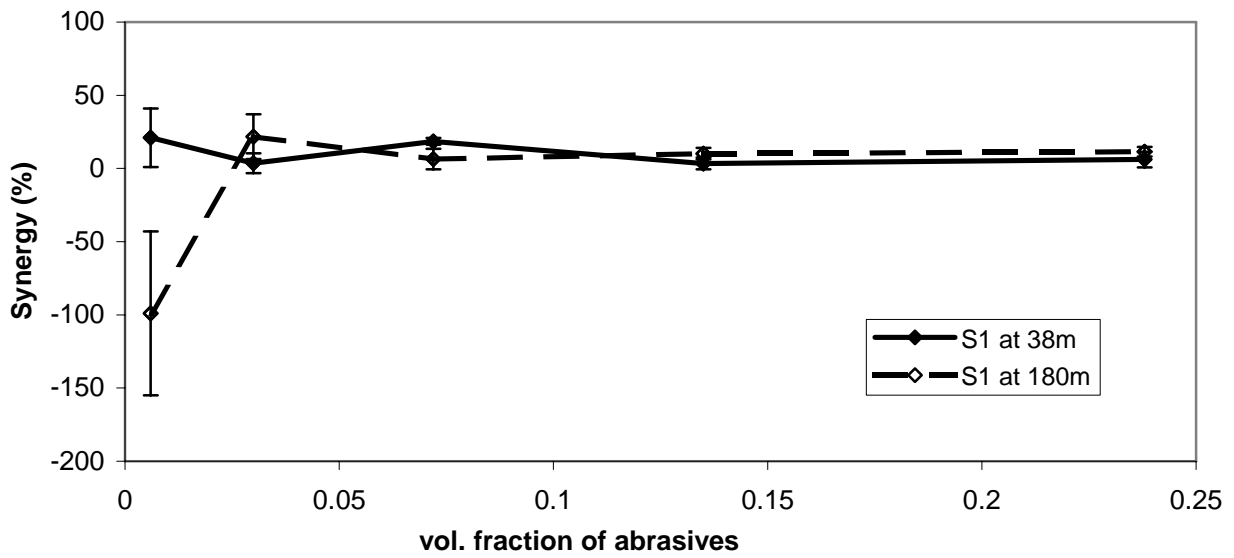


**Figure 11:** Direct comparison of  $S_1$  for AISI 316L at both 38 and 180 m.

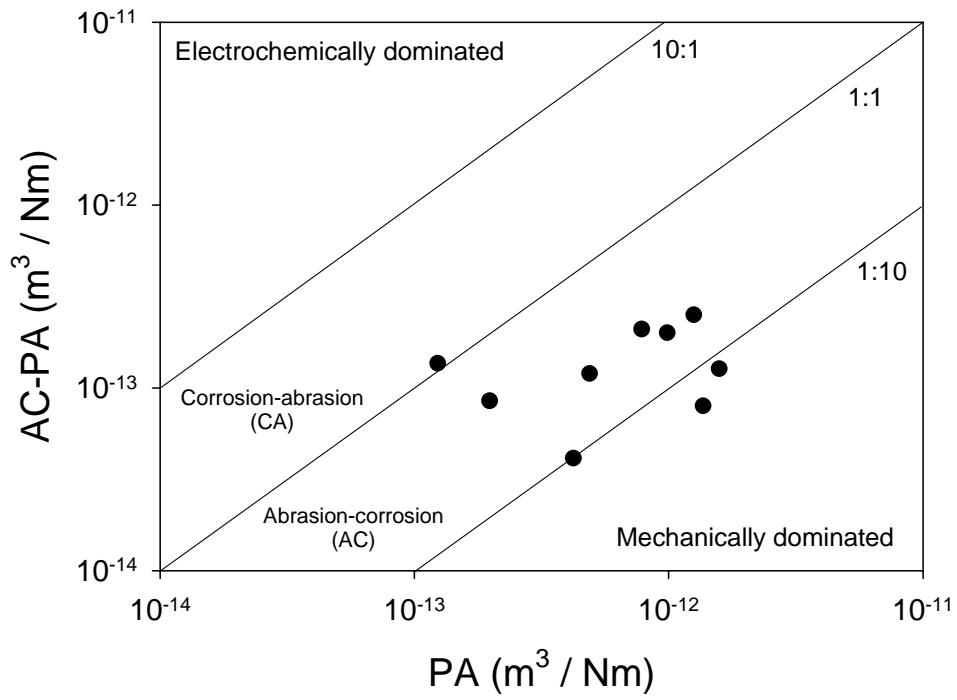


**Figure 12:** Abrasion-corrosion mechanism map for AISI 316L. Lines indicate AC-PA / PA ratios of 10:1, 1:1 and 1:10.